Microfluid Nanofluid (2016) 20:70
DOI 10.1007/s10404-016-1731-4

RESEARCH PAPER

# Microfluidic mixing using pulsating flows

**Farah Cheaib[1] · Gacia Kekejian[1] · Sylvie Antoun[1] · Mohammad Cheikh[1] · Issam Lakkis[1]**

Received: 5 October 2015 / Accepted: 15 March 2016 / Published online: 16 April 2016


**Abstract** Mixing of biological species in microfluidic channels is challenging since the mixing process is limited by the small mass diffusion coefficient of the species and by the dominance of viscous effects, captured by the low value of Reynolds number characteristic of laminar liquid flow in microchannels. This paper investigates the use of pulsating flows to enhance mixing in microflows. The dependence of the degree of mixing on various dimensionless groups is investigated. These dimensionless numbers are Strouhal number, pulse amplitude divided by base velocity, Reynolds number, location along the mixing channel normalized by the channel width, channel cross section aspect ratio, and phase difference between the inlet streams. The degree of mixing, observed to experience both spatial fluctuations down the mixing channel and temporal fluctuations over a pulsation cycle at the quasi-stationary state, is shown to be most sensitive to changes in pulsation amplitude and frequency. For a fixed pulsation amplitude and Reynolds number, the degree of mixing has a peak value for a certain Strouhal number above and below which the degree of mixing decreases. Increasing the pulsation amplitude improves mixing with the behavior becoming asymptotic at large pulsation amplitudes. The temporal fluctuations in the degree of mixing over a cycle at the quasi-stationary state decrease and the average degree of mixing increases downstream the mixing channel. The fluctuations are also smaller at higher values of the Strouhal number and are generally larger for larger pulsation amplitudes. This study also takes into account the rate of work input required to overcome viscous effects. While this power input is independent of the pulsation frequency, it exhibits a parabolic dependence on the pulsation amplitude. Finally, considering the dependence of the degree of mixing (mean and standard deviation), mixing length, and energy consumption on these dimensionless groups, examples of the trade-off that has to be made in choosing the operating conditions based on different constraints are presented.

**Keywords** Microfluidic mixing · Pulsating flows · More

**List of symbols**

| | |
|---|---|
| $A$ | Channel cross-sectional area |
| $c$ | Concentration of a species |
| $\overline{c}$ | Reference concentration |
| $D$ | Mass diffusivity |
| $E$ | Total energy |
| $f$ | Pulsation frequency |
| $h$ | Enthalpy |
| $H$ | Channel height (or depth) |
| $L$ | Channel length |
| $\dot{m}$ | Mass flow rate |
| $p$ | Pressure |
| $Q$ | Volume flow rate |
| $\overline{Q}$ | Base volume flow rate |
| $R$ | Channel resistance |
| $t$ | Time |
| $T$ | Pulsation period |
| $U$ | Characteristic speed |
| $V$ | Average velocity |
| $\overline{V}$ | Base/mean velocity |
| $\mathbf{v}$ | Velocity vector $(v_x, v_y, v_z)$ |
| $W$ | Channel width |
| $W_{v,\text{cycle}}$ | Work input to overcome friction during a cycle |
| $x$ | Coordinate along the mixing channel |

✉ Issam Lakkis
ilakkis@gmail.com

[1] American University of Beirut, Beirut, Lebanon

| | |
|---|---|
| $y$ | Coordinate along channel width |
| $z$ | Coordinate along channel height |
| $Re$ | Reynolds number |
| $Pe$ | Peclet number |
| $St$ | Strouhal number |
| $Sc$ | Schmidt number |
| $\alpha$ | Angle between the two inlet channels |
| $\beta$ | Channel resistance correction factor |
| $\delta V$ | Amplitude of pulsed velocity |
| $\delta Q$ | Pulsation volume flow rate |
| $\gamma$ | Channel cross section aspect ratio |
| $\kappa$ | Kinetic energy correction factor |
| $\overline{\mu}$ | Average degree of mixing |
| $\eta$ | Dynamic viscosity |
| $\nu$ | Kinematic viscosity |
| $\omega$ | Angular velocity |
| $\phi$ | Phase difference |
| $\rho$ | Density |
| $\sigma_\mu$ | standard deviation in degree of mixing |
| $\theta$ | Ratio of channel width to length |
| $\xi$ | Mass fraction of a species |
| $\xi$max | Mass fraction at perfect mixing |

**Superscripts**

| | |
|---|---|
| * | For dimensionless variables |

**Subscripts**

| | |
|---|---|
| 1 | For inlet channel 1 |
| 2 | For inlet channel 2 |
| 3 | For mixing channel |

## 1 Introduction

With the advancements of technology, microfluidics is witnessing huge progress and showing impressive potential. Micro total analysis systems or lab-on-a-chip devices and DNA/protein microarrays are practical examples of microfluidic applications in clinical diagnostics, drug discovery and delivery, flow chemistry etc. Engineering applications of microfluidics face several challenges such as manufacturing techniques, flow control, and mixing (Lim et al. 2010; Karniadakis et al. 2006).

Mixing, in particular, is very important in microfluidic applications (Stone et al. 2004) since good mixing needs to be achieved within an acceptable time range, a reasonable channel length, and at an affordable power consumption. Mixing in microchannels can be challenging primarily due to the small value of the mass diffusion coefficient of the species to be mixed, in addition to the fact that the flow is laminar and in many cases nearly inertia-free. Mixing of fluids in microchannels is extensively investigated in literature and many methods of mixing are presented. These methods for mixing can be divided into two main categories: passive and active (Lim et al. 2010; Hessel et al. 2005; Capretto et al. 2011). Unlike active mixing, passive mixing does not involve an external driving force (Lim et al. 2010); instead, it is done, for example, by changing the geometry of the channel, inserting microgrooves (Du and Manoochehri 2010) or ribs (Goullet et al. 2006) in the channel, hydrodynamic mixing (Knight et al. 1998), or distributive mixing (Bessoth 1999). While these methods enhance mixing by introducing instabilities that increase the interface between the two fluids, it is usually hard to manufacture such channels due to the complexities of the geometry. Active mixing such as electro osmosis (Chang and Yang 2007), electrostatic mixing (Patrascu et al. 2012), and micromagnetic stir-bar mixers (Lu et al. 2002) require external fields, energy, and additional components to enhance mixing. These additional components can make the mixing device bulky (Lim et al. 2010).

This paper discusses mixing of two streams using time pulsing, i.e., varying the flow rate of each of the inlet channels periodically with time. In a series of papers, (Glasgow and Aubry 2003; Glasgow et al. 2004; Goullet et al. 2005, 2006) studied microfluidic mixing using time pulsing by evaluating the degree of mixing at a certain distance after the confluence region. In this work mixing with pulsating flows is further investigated by varying key dimensionless parameters and studying their effect on the mixing process, new results are presented and previous ones are corrected.

Goullet et al. (2005, 2006), Glasgow et al. (2004), and Glasgow and Aubry (2003) previously studied mixing using time pulsing in several channel geometries with a focus on mixing in a T channel configuration and in a perpendicular $\perp$ channel configuration shown in Fig. 1.

Their results show that pulsing can be an effective method for mixing, as quantified by the degree of mixing expressed as

$$\overline{\mu} = 1 - \sqrt{\frac{\int_A (\xi - \xi_{\max})^2 \mathbf{v} \cdot \hat{n}\, dA}{\int_A \xi_{\max}^2 \mathbf{v} \cdot \hat{n}\, dA}} \tag{1}$$

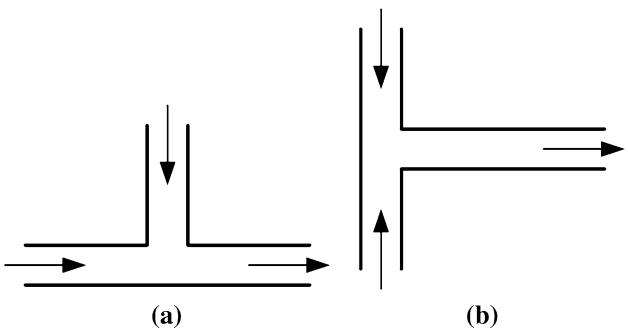


**Fig. 1** Channel configurations (Goullet et al. 2006). **a** Perpendicular $\perp$ channel. **b** T channel

where $A$ is the channel cross section, $\hat{n}$ is the unit vector normal to d$A$, $\mathbf{v}$ is the velocity vector, $\xi$ is the mass fraction, and $\xi_{\max}$ is mass fraction of perfect mixing ($\xi_{\max} = 0.5$). Note that a degree of mixing of one denotes complete mixing and a degree of mixing of zero indicates no mixing. Based on Eq. (1), the degree of mixing is numerically computed as

$$\overline{\mu} \simeq 1 - \sqrt{\frac{\sum_{i=1}^{n} (\xi - \xi_{\max})^2 v_i A_i}{\sum_{i=1}^{n} \xi_{\max}^2 v_i A_i}} \tag{2}$$

where the cross-sectional area $A$ is discretized as $n$ grid cells, $A_i$ is the area of grid cell $i$, $\xi_i$ and $v_i$ are respectively the mass fraction and velocity component normal to $A_i$ at the $i$th cell.

CFD simulations (Goullet et al. 2005; Glasgow and Aubry 2003) were carried out in the perpendicular channel and the T channel for the following flow configurations (1) constant flows from both channels, (2) pulsed flows from both channels, and (3) pulsed flows from one channel. Some of these simulations were also repeated in ribbed channels to find the effects of ribs on mixing. The pulsing is achieved by imposing a velocity of the form $\overline{V} + \delta V \sin(2\pi f t + \phi)$ at the inlets where $\overline{V}, \delta V, f$, and $\phi$ are respectively the mean velocity, the pulse amplitude, the pulse frequency, and the phase. The main findings (Goullet et al. 2005, 2006; Glasgow et al. 2004; Glasgow and Aubry 2003) are (1) using constant flows in channels results in a much lower degree of mixing than pulsating flows, (2) pulsing the flows from both inlets with a 90° phase shift yields the highest degree of mixing of $\overline{\mu} = 0.59$ in a perpendicular channel and $\overline{\mu} = 0.66$ in a T channel, (3) using a ribbed channel, the degree of mixing increased to 0.78 in the perpendicular channel, (4) increasing the Strouhal number (pulsation frequency) improves mixing, (5) increasing the pulse volume ratio (ratio of pulse volume to the intersection volume) improves mixing, (6) a higher pulsing amplitude improves mixing.

The results (Goullet et al. 2005, 2006; Glasgow et al. 2004; Glasgow and Aubry 2003), however, do not account for certain factors in pulsating flows which can significantly influence the results. The settings and factors that are taken into consideration in the simulations presented in this paper to ensure reliable results, are (1) running the transient simulations for a sufficiently long time to ensure that the pulsating flow reaches a quasi-stationary state, choosing (2) appropriately sized time steps, (3) sufficient channel length, and (4) sufficiently small mesh sizes. The degree of mixing at closely spaced cross sections along the mixing channel is recorded at every time step and accurate description of the behavioral dependence of the degree of mixing on dimensionless groups is ensured by sufficiently resolving their ranges of interest. Other aspects of the numerical solver are (1) using double precision computations, (2) pressure based with pressure-velocity coupling, (3) spatial discretization: second-order pressure, second-order upwind momentum and species, and (4) second-order implicit in time.

The significance of this work then lies in clearly outlining the factors that should be taken into consideration when studying pulsating flows. Based on these factors, the problems with the previous results by Glasgow et al. (2004), Glasgow and Aubry (2003), and Goullet et al. (2005, 2006), are clarified, and gaps are filled in. This paper also expands the study of pulsating flows to sweep a range of values of Strouhal numbers and pulsing amplitudes to more clearly and accurately capture the effect of these numbers on mixing. This study also investigates the effects of the fluid viscosity, of the phase difference between the two pulsating streams, and of the channel cross section aspect ratio.

This paper is organized as follows. First, the problem is stated and the criteria for good mixing is outlined. Second, the governing equations are presented along with the various dimensionless groups. Discussion of work needed for mixing follows. Computational aspects are then discussed followed by a presentation and discussion of the results.

## 2 Problem statement

In this work the use of pulsating flows to achieve mixing is investigated in terms of the degree of mixing, mixing length, and energy requirements. The general configuration and parameters shown in Fig. 2 are considered, where $H$ is the channel height (or depth) ($H = \infty$ for most of the simulations since 2D simulations were mostly run), $W = 200\,\mu$m is the channel width, $L_1$ is the length of each of the inlet fluid channels, $\alpha = 180°$ is the angle between the two inlet channels, and $L$ is the length of the mixing channel.

The effects of Strouhal number ($St$), ratio of amplitude/base velocity ($\delta V/\overline{V}$), channel cross section aspect ratio

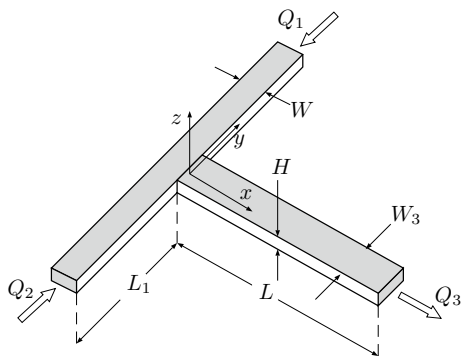


**Fig. 2** Schematic and dimensions

($W/H$), Reynolds number ($Re$), and phase difference ($\phi$) are closely studied, considering:

1. The degree of mixing, taking into account both its temporal average as well as fluctuations over a cycle under quasi-periodic conditions.
2. The mixing length; the location down the mixing channel at which a minimum desired degree of mixing and a maximum allowable fluctuation amplitude is achieved.
3. The energy needed to achieve a particular degree of mixing at a certain location for the studied cases.

Based on these criteria, the best scenario is that which yields highest degree of mixing with minimum fluctuations, consumes the least energy, and uses the smallest mixing length.

## 3 Governing equations and dimensionless groups

The volume flow rates of the two streams to be mixed are respectively $Q_1(t) = \overline{Q} + \delta Q \sin(2\pi ft)$ and $Q_2(t) = \overline{Q} + \delta Q \sin(2\pi ft + \phi)$, where $f$ is the pulsing frequency and $\phi$ is the phase shift between the two flows. Since the cross-sectional areas are constant, the corresponding average velocities are $V_1(t) = \overline{V} + \delta V \sin(2\pi ft)$ and $V_2(t) = \overline{V} + \delta V \sin(2\pi ft + \phi)$, with $\overline{V} = \overline{Q}/A$, $A = WH$ and $\delta V = \delta Q/A$. The flowrate in the mixing channel is $Q_1(t) + Q_2(t) = 2\overline{Q} + \delta Q(\sin(2\pi ft) + \sin(2\pi ft + \phi))$. Note that the flow rate in the mixing channel, averaged over one pulsation cycle, is $2\overline{V}A$.

To non-dimensionalize the governing equations, the velocity, length, time, pressure, and species concentration are scaled as follows:

$$\mathbf{v}^* = \frac{\mathbf{v}}{U},\ x^* = \frac{x}{L},\ y^* = \frac{y}{W},\ z^* = \frac{z}{H},\ t^* = tf,$$
$$p^* = \frac{p}{\eta UL/W^2},\ c^* = \frac{c}{\overline{c}} \tag{3}$$

where the characteristic speed $U$ is chosen to be the average speed in the mixing channel, $U = 2\overline{V}W/W_3$.

For the rest of the section, the governing equations are presented in dimensionless form for parallel flow in the $x$ -direction along the channel, i.e., $\mathbf{v} = (v_x, 0, 0)$. For simplicity, the star superscript will be removed. Note that the pressure scale is picked by balancing the pressure gradient along the channel with the dominant viscous term of the momentum equation for $H \gg W$.

### 3.1 Continuity equation

For incompressible flow, the conservation of mass, expressed in dimensionless form, is

$$\frac{\partial v_x}{\partial x} + \frac{\partial v_y}{\partial y} + \frac{\partial v_z}{\partial z} = 0 \tag{4}$$

If the flow is parallel to the $x$-direction, then $v_y^* = v_z^* = 0$, it follows that $\partial v_x{}^*/\partial x^* = 0$ and, from the $y$ and $z$ components of the momentum equation, that $p^*$ is a function of $x^*$ and $t^*$ only.

### 3.2 Momentum equation

For $W \ll L$, $\left|\frac{\partial^2 v_x}{\partial x^2}\right| / \left|\frac{\partial^2 v_x}{\partial y^2}\right| \sim (W/L)^2$ and the momentum equation in the flow, in dimensionless form, is approximated as

$$St\, Re \frac{\partial v_x}{\partial t} = -\frac{\partial p}{\partial x} + \frac{\partial^2 v_x}{\partial y^2} + \gamma^2 \frac{\partial^2 v_x}{\partial z^2} \tag{5}$$

where $\gamma = \frac{W}{H}$, $St = \frac{fW}{U}$ is the Strouhal number and $Re = \frac{UW}{\nu}$ is the Reynolds number; $\nu = \eta/\rho$ is the kinematic viscosity. In the mixing channel $W = W_3$, $H = H_3$, and $U = 2\overline{V}W/W_3$.

The solution of Eq. (5) can be expressed as Lakkis (2008)

$$v_x(\mathbf{x}, t) = -\frac{16}{ReSt} \sum_{m=0}^{\infty} \sum_{n=0}^{\infty} \frac{\sin(\beta_m y) \sin(\nu_n z)}{\beta_m \nu_n} \times \int_0^t e^{-\frac{\beta_m^2 + \gamma^2 \nu_n^2}{ReSt}(t-\tau)} \frac{\partial p(x,\tau)}{\partial x} \mathrm{d}\tau \tag{6}$$

where $\beta_m = (2m+1)\pi$, $\nu_n = (2n+1)\pi$.

### 3.3 Mass transfer equation

The mass transfer equation, expressed in dimensionless form, is

$$St \frac{\partial c}{\partial t} + \theta\, v_x \frac{\partial c}{\partial x} = \frac{1}{Pe}\left(\frac{\partial^2 c}{\partial y^2} + \gamma^2 \frac{\partial^2 c}{\partial z^2}\right) \tag{7}$$

where $c$ is the species concentration, $\theta = \frac{W}{L}$, and Peclet number $Pe = \frac{UW}{D}$ may be expressed as the product of Reynolds and Schmidt number $Pe = Sc \cdot Re$, with $Sc = \frac{\nu}{D}$.

Finally, the dimensionless numbers that will be used in the analysis are $\alpha = 180°$, $\phi$, $St$, $Re$, $Pe$, $\frac{\delta V}{\overline{V}}$, $\gamma$, and $\theta$.

## 4 Energy analysis

In this section, the energy consumption per cycle of this mixing device is determined in terms of the frequency, phase angle, mean velocity and amplitude velocity. The energy cost per cycle, being one of the performance measures outlined earlier, serves as a basis for comparing

various mixing scenarios as well as for comparison with other conventional mixing techniques.

Applying the first Law of Thermodynamics on the control volume of Fig. 2, assuming adiabatic conditions, and noting that the $pdV$ work is zero, then

$$\frac{\partial E}{\partial t} + \int_{CS} \rho\left(h + \frac{1}{2}|\mathbf{v}|^2\right)\mathbf{v}\cdot\hat{n}\,dA = -\dot{W}_v \tag{8}$$

Neglecting change in internal energy due to viscous heating, we get

$$\frac{\partial E}{\partial t} + \dot{W}_v = Q_1\left(P_1 + \frac{\kappa_1}{2}\rho V_1^2\right) + Q_2\left(P_2 + \frac{\kappa_2}{2}\rho V_2^2\right) - Q_3\left(P_3 + \frac{\kappa_3}{2}\rho V_3^2\right) \tag{9}$$

where $\dot{W}_v$ is the rate of work done by the fluid to overcome viscous forces, and $\kappa$ is the kinetic energy correction factor. From the mass conservation equation $Q_3 = Q_1 + Q_2$, then, $V_3 = (V_1A_1 + V_2A_2)/A_3$ where $V_1 = \overline{V} + \delta V \sin(\omega t)$ and $V_2 = \overline{V} + \delta V \sin(\omega t + \phi)$.

It has been shown (Lakkis 2008; Issa 2015), based on Eq. (6), that a reduced-order circuit model of unsteady incompressible flow in a rectangular channel consists of an infinite number of parallel branches, where each branch consists of an inductor in series with a resistance. Since the inductor is a reactive element, it does not dissipate energy, and it can be shown that the energy dissipated over a pulsation cycle is due to the total (viscous) resistance ($R = \Delta P/Q$) of the parallel branches. To compute the energy dissipated over a pulsation cycle, the reduced-order circuit model shown in Fig. 3 is used, where $R_1$ is the resistance of channel inlet 1, $R_2$ is the resistance of channel inlet 2, $R_3$ is the resistance from the beginning of the mixing channel to location $x_3$, and $R_4$ is the resistance of the mixing channel from location $x_3$ to the outlet.

Assuming the inlet channels are identical and that all the channels have the same height, $H$, then

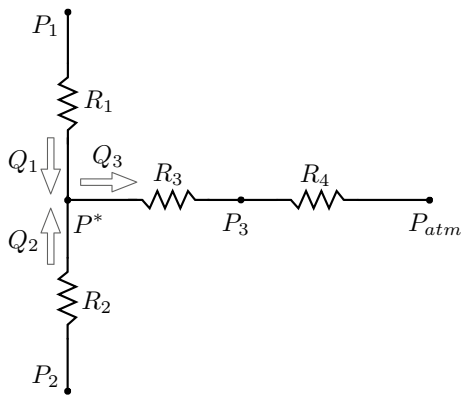


**Fig. 3** Reduced-order circuit model of the mixer

$$R_1 = R_2 = \frac{12\eta L_1}{HW_1^3}\frac{1}{\beta_1}, \quad R_3 = \frac{12\eta L_3}{HW_3^3}\frac{1}{\beta_3}, \quad R_4 = \frac{12\eta L_4}{HW_3^3}\frac{1}{\beta_3} \tag{10}$$

where, for $\gamma \leq 1$,

$$\beta = 1 - \frac{192\gamma}{\pi^5}\sum_{n=0}^{\infty}\frac{\tan h\left(\frac{(2n+1)\pi}{2\gamma}\right)}{(2n+1)^5}, \tag{11}$$

with $\beta \simeq 1$ for $\gamma \ll 1$. Equation 9 can then be integrated in time over 1 period ($T = 1/f$), giving the following expression for the (normalized) rate of work input required to overcome friction

$$\frac{W_{v,\text{cycle}}St}{\rho HW_1^2\overline{V}^2} = \frac{12}{\theta_1\beta_1 Re}\left[\left(\frac{\gamma_3^2}{\gamma_1^2} + \frac{\theta_1\beta_1}{\theta_3\beta_3}\right)\left(\frac{\delta V}{\overline{V}}\right)^2 + \left(2\frac{\gamma_3^2}{\gamma_1^2} + 4\frac{\theta_1\beta_1}{\theta_3\beta_3}\right)\right] - \kappa_1\left[\left(\frac{3}{2}\frac{\kappa_3}{\kappa_1} - \frac{3}{4}\frac{\gamma_3^2}{\gamma_1^2}\right)\left(\frac{\delta V}{\overline{V}}\right)^2 + 2\frac{\kappa_3}{\kappa_1} - \frac{1}{2}\frac{\gamma_3^2}{\gamma_1^2}\right] \tag{12}$$

For $W_1 = W_3$, $\theta_1/\theta_3 = L_3/L$, $U = 2\overline{V}$, $\kappa_1 = \kappa_3$, $\beta_1 = \beta_3$ can be approximated as $\beta \simeq 0.9893 - 0.59\gamma$ (with a relative error <5 %), we get

$$\frac{W_{v,\text{cycle}}St}{\rho HW_1^2\overline{V}^2} = \frac{12}{\beta\theta Re}\left[\left(1 + \frac{L_3}{L}\right)\left(\frac{\delta V}{\overline{V}}\right)^2 + 2 + 4\frac{L_3}{L}\right] - \frac{3}{2}\kappa\left(1 + \frac{1}{2}\left(\frac{\delta V}{\overline{V}}\right)^2\right) \tag{13}$$

By inspecting Eq. (13), one can see that for a fixed geometry, a given fluid, and fixed average velocity $\overline{V}$, the product $W_{v,\text{cycle}}St$ depends on (1) the length of the mixing channel $L_3$, (2) the inverse of Reynolds number and (3) on the square of the pulsation amplitude. Note that the kinetic energy recovery term on the right-hand side of Eq. (13) is negligible (when compared to the viscous term) when the flow inertia is small, i.e., for $Re\frac{W}{L} \ll 1$.

In what follows, a computational study is carried out to investigate the impact of the dimensionless variables, introduced in Sect. 3, on mixing. To this end, numerical simulations of the unsteady Navier–Stokes and species transport equations for laminar flows in two and three-dimensional coordinates were carried out using FLUENT/ANSYS.

## 5 Computational procedure and validation

Computational fluid dynamics (CFD) simulations on FLUENT/ANSYS were carried out for the T geometry previously used in the literature (Glasgow et al. 2004; Goullet et al. 2005, 2006) and shown in Figs. 1b and 2 with $\alpha = 180°$, $W = 200\,\mu\text{m}$, $H/W = 1, 2$, and $\infty$. In the CFD simulations, the two velocity inlets are assigned velocities

$V = \overline{V} + \delta V \sin(2\pi ft)$ and $V = \overline{V} + \delta V \sin(2\pi ft + \phi)$ respectively. The exit of the mixing channel is set as a pressure outlet. The fluids entering from both inlets have identical properties but are simply named differently to allow the observation of diffusion. Due to symmetry with respect to the $xy$ plane, only half of the domain is considered. The working fluid is chosen to be water; the density is set at $\rho = 1000\,\mathrm{kg/m^3}$ and the dynamic viscosity for all simulations is set at $\eta = 0.001\,\mathrm{kg/ms}$ (except for the simulations with a higher reynolds number where $\eta$ was modified). The diffusion coefficient of the species to be mixed is chosen to be $D = 10^{-10}\,\mathrm{m^2/s}$, which is within the range of diffusion coefficients of biomolecules in water Atkins and De Paula (2010). The corresponding Schmidt number is $Sc = 10{,}000$.

In order to accurately capture the behavior in the mixing channel, the effect of several factors on the results were closely observed. These factors include (1) number of time steps per cycle, (2) mesh size, (3) length of the inlet and mixing channels, and (4) the time at which results are recorded. Unless otherwise specified, the Strouhal number and Reynolds numbers presented in the results are $St = fW/\overline{V}$ and $Re = \overline{V}W/\nu$. These expressions correspond to a characteristic speed equal to the average speed in the mixing channel $U = 2\overline{V}$ and to a characteristic length equal to the hydraulic diameter of a channel of infinite height ($H/W \to \infty$); $D_h = 2W$.

### 5.1 Impact of time step

To observe the effect of the time step size on the results, a 2D simulation with $\delta V/\overline{V} = 5$, $W = 200\,\mu\mathrm{m}$, $\phi = 90°$, and $St = 1.5$ was carried out with the following values for the number of time steps per pulsation cycle: 20, 40, 80, 160, and 320. The mesh size used is $\Delta x = 10\,\mu\mathrm{m}$. Figure 4 shows that varying $N$ can significantly influence results. The difference between the results is most significant between $x/W = 1$ and $x/W = 6$ with results becoming closer at the beginning and end of the channel. It can also be observed that using large time steps leads to significant over-prediction of the degree of mixing, as a consequence of not sufficiently resolving the pulsation cycle. Based on these results the number of time steps per cycle used in the simulations was set at 160, the value at which the results with respect to number of time steps converged.

### 5.2 Impact of mesh size

The effect of the mesh size was also taken into consideration and found to have a significant influence on the degree of mixing for the 2D case with $W = 200\,\mu\mathrm{m}$, $\overline{V} = 0.001\,\mathrm{m/s}$, $\delta V/\overline{V} = 5$, $\phi = 90°$, and $St = 1.5$. Figure 5 shows the variation of the degree of mixing with decreasing mesh sizes. Larger mesh sizes yield inaccurately higher degrees of mixing. Convergence of results with respect to mesh size was found to be at a mesh size with $\Delta x = 5\,\mu\mathrm{m}$ and so this value of mesh size was chosen for the simulations performed.

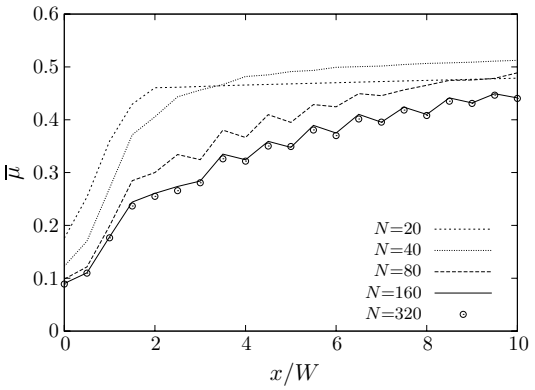


**Fig. 4** Impact of time step on average degree of mixing along the mixing channel

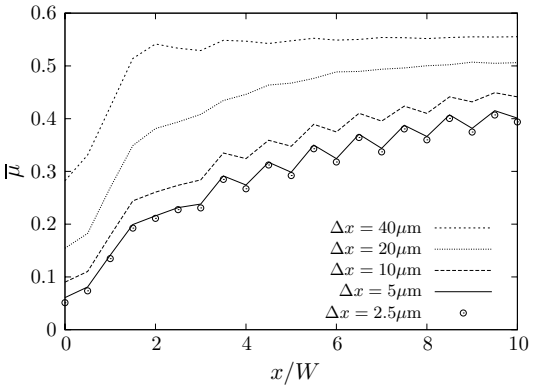


**Fig. 5** Impact of mesh size on average degree of mixing along the mixing channel

### 5.3 Quasi-stationary state

The results presented in this paper are all recorded at the quasi-stationary state, when the solution no longer varies between subsequent cycles. This implies that each simulation must run for a sufficiently long time to reach the quasi-stationary state. Of importance also is the minimum mixing length, defined as the distance from the mixing channel entrance where the flow, once it has reached the quasi-stationary state, experiences temporal fluctuations in the degree of mixing with a variance less than a desired threshold value.

To illustrate these points, the case with $V_1 = 0.001 + 0.0075\sin(10\pi t)$ and $V_2 = 0.001 + 0.0075\sin(10\pi t + \pi/2)\,\mathrm{m/s}$ is simulated. Figure 6 shows the

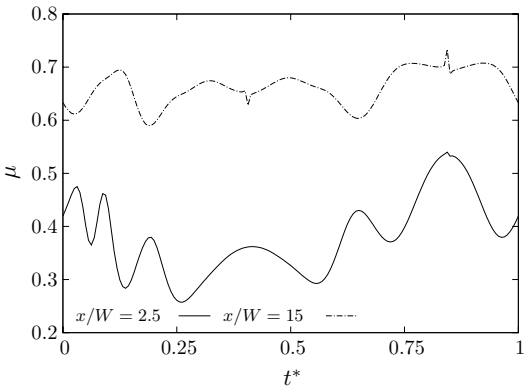


**Fig. 6** Degree of mixing over a cycle at the quasi-stationary state at two locations down the mixing channel

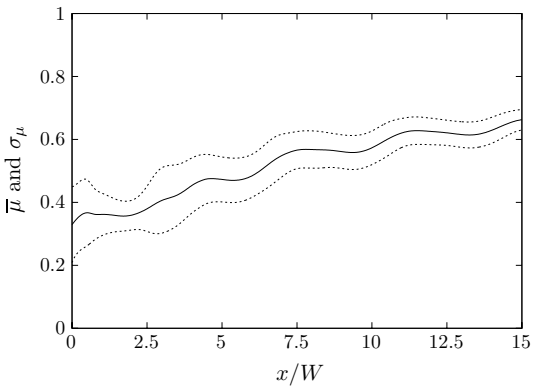


**Fig. 7** Average degree of mixing and standard deviation versus location down the mixing channel at quasi-stationary state

fluctuations in the degree of mixing experienced by the flow over one cycle at positions $x/W = 2.5$ and $x/W = 15$. The degree of mixing experiences more and larger fluctuations at the location ($x/W = 2.5$) closer to the mixing channel entrance than farther down ($x/W = 15$). This is confirmed in Fig. 7, where the degree of mixing ($\overline{\mu}$), averaged over one cycle at the quasi-stationary state, is plotted against the distance from the mixing channel entrance. The dashed lines in the plot correspond to $\overline{\mu} + \sigma_\mu$ and $\overline{\mu} - \sigma_\mu$, where $\sigma_\mu$ is the standard deviation of the temporal fluctuations over a cycle at the quasi-stationary state at a given location. So the distance between the dashed lines for a given location ($x/W$) provides a measure of the peak to peak temporal variations over a cycle at that location.

It can be observed from Fig. 7 that the average degree of mixing continues to increase down the channel due to mass diffusion across the interface between the streams. It can also be observed that the temporal fluctuations in the degree of mixing decreases down the channel. This can be attributed to the role of viscous effects in damping these fluctuations. Thus a smaller minimum mixing length is accompanied by a larger threshold standard deviation and vice versa, For example, a threshold fluctuations standard deviation of 0.05 corresponds to a minimum mixing length of 10.75 $W$ while a threshold fluctuations standard deviation of 0.075 correspond to a minimum mixing length of 4.65 $W$. The corresponding values of the average degree of mixing at these two locations are 0.61 and 0.475.

Figures 6 and 7 show that the time and location at which results are recorded is important and can alter results. As an example of the discrepancy in the results that may arise if certain simulation parameters are not closely taken into consideration, the following case of mixing in a three-dimensional T configuration is presented: $W = 200\,\mu\text{m}$, $H = 120\,\mu\text{m}$, $f = 5\,\text{Hz}$, $\delta V/\overline{V} = 7.5$, $V = 0.001\,\text{m/s}$, and $\phi = 90°$. This case was presented by Glasgow et al. (2004), Goullet et al. (2005), where the recorded degree of mixing was shown to be 0.66 at the position of $x/W = 2.5$ after 2s of flow time. The number time steps per cycle was taken to be 40, and the model is a 3D model with a hexahedral mesh, where most of the cells have a side length of $10\,\mu\text{m}$ Goullet et al. (2005). Simulating the same case, but with the considerations presented and studied earlier taken into account, yielded an average degree of mixing obtained of 0.4 at the same location used in Goullet et al. (2005). Based on the analysis previously presented the result obtained in Goullet et al. (2005) overestimates the mixing due to the lower number of time steps, the bigger mesh size, and the time of recording of the result.

### 5.4 Length of channels

At the end of the channel a drop in the degree of mixing is always seen to extend over a certain length. This is an end effect due to back flow and to the boundary conditions imposed at the end of the mixing channel. To avoid having these end effects interfering with the recorded results, it was always made sure that the exit channel is appended by an artificial section of length exceeding the distance traveled in reverse by the flow up the mixing channel during a period, so that during flow reversal over the second half of the period the flow entering through the mixing channel exit occupies this extension only without contaminating the main section of the mixing channel.

The length of the inlet channels is also chosen to exceed the distance the flow travels in reverse during a period as well so that the inlet boundary conditions are respected.

### 5.5 Verification of the viscous work

The pressure calculated through the equation $\Delta P = R \cdot Q$ was compared against the numerical values of the pressure obtained from the simulations on FLUENT/ANSYS to further validate the energy calculations. The two pressures, that

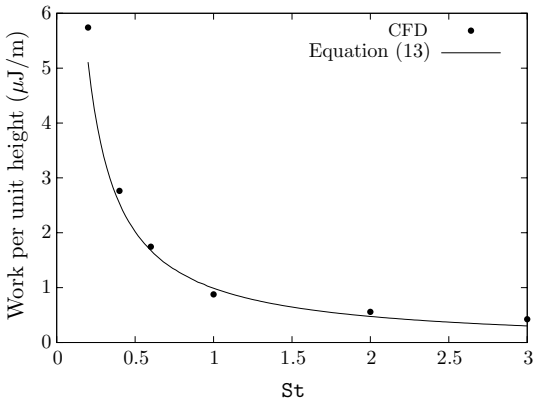


**Fig. 8** Comparison between numerical simulation (*symbols*) and Eq. (13) (*solid line*)

**Table 1** Varying $\delta V/\overline{V}$ at $St = 2$

| $\delta V/\overline{V}$ | $\overline{V}$ (m/s) | $\delta V$ (m/s) |
|---|---|---|
| 0 | 0.001 | 0 |
| 2.5 | 0.001 | 0.0025 |
| 3.75 | 0.001 | 0.00375 |
| 5 | 0.001 | 0.005 |
| 6.25 | 0.001 | 0.0075 |
| 7.5 | 0.001 | 0.0075 |
| 10 | 0.001 | 0.01 |

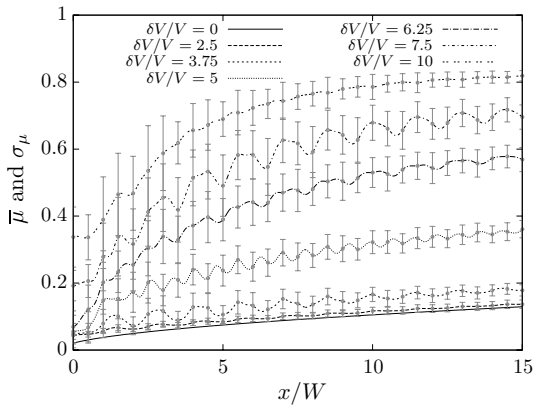


**Fig. 9** Average degree of mixing and the standard deviation versus $x$ / $W$ for $\delta V/\overline{V} = 0, 2.5, 3.75, 5, 6.25, 7.5, 10$ for $St = 2$

obtained from the resistance formula, and that obtained from simulations, proved to be very similar, especially in the cases where inertia effects are weak ($\theta Re \ll 1$). The comparison of the work input per unit height ($H$) per cycle required to overcome friction over a mixing channel of 2000 μm length with $\delta V/\overline{V} = 5$, presented in Fig. 8, shows that Eq. (13) is valid for the range of values of Strouhal number of interest.

## 6 Results and discussion

In this section, the impact of pulsation amplitude ($\delta V/\overline{V}$), pulsation frequency ($St$), Reynolds number ($Re$), phase difference ($\phi$), and channel cross section aspect ratio ($H$ / $W$) on mixing is numerically investigated. For all the simulations presented, and unless otherwise specified, the following dimensionless parameters are kept constant: $\alpha = 180°$, $Re = 0.2$, and $\phi = 90°$. For every group of simulations, one dimensionless group is varied (while the others kept fixed) and the results are recorded on planes placed every 50 μm down the mixing channel. The degree of mixing is then recorded at these discrete locations during one stationary cycle. The mean and standard deviation of the degree of mixing during one cycle are then computed; these values are used to make the plots in the following sections.

In the low $Re$ flow regime, when the pulsating frequency is small ($f < \overline{V}/W$), the role of inertia in the momentum equation is small ($Re < 1$ and $Re \cdot St < 1$) and the velocity profile approaches the Poiseuille profile. In the mass transfer equation, advection dominates diffusion due to the

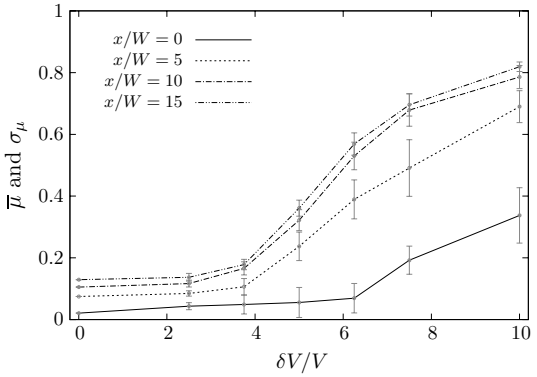


**Fig. 10** Average degree of mixing and the standard deviation versus $\delta V/\overline{V}$ at $x/W = 5, 10$ and 15 for $St = 2$

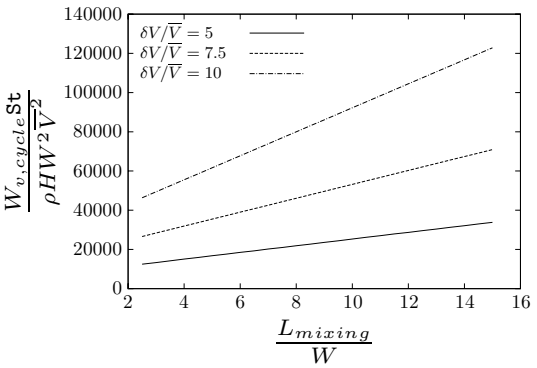


**Fig. 11** Normalized energy consumption as a function of mixing length and pulsation amplitude

**Table 2** Varying Strouhal number at $Re = 0.2$

| $St$ | Frequency $f$ | $\delta V/\overline{V}$ |
|---|---|---|
| 0.1 | 0.5 | 5, 7.5, 10 |
| 0.2 | 1 | 5, 7.5, 10 |
| 0.4 | 2 | 5, 7.5, 10 |
| 0.6 | 3 | 5, 7.5, 10 |
| 0.8 | 4 | 5, 7.5, 10 |
| 1 | 5 | 5, 7.5, 10 |
| 1.5 | 7.5 | 5, 7.5, 10 |
| 2 | 10 | 5, 7.5, 10 |
| 3 | 15 | 5, 7.5, 10 |
| 4 | 20 | 5, 7.5, 10 |

small value of the mass diffusion coefficient. When the two low inertia streams meet, mixing takes place as diffusion across the interface. In this diffusion limited regime, the transverse diffusion length scales as $\delta(x) \sim \sqrt{Dx/\overline{V}}$ so that the channel length required for diffusion across the channel, starting at the centerline, to reach the channel wall is $L^* \sim Pe\, W$, where $Pe = Re \cdot Sc$, $Sc = 10^4$ and $Re = O(1)$. As a result, the degree of mixing is very low (Goullet et al. 2006) for mixing channels of length $L << L^*$.

Pulsating flows improve mixing by significantly increasing the length of the interface between the two streams across which mixing takes place by diffusion. This increase in the interface length is due to the winding caused by the pulsating streams with 90° phase difference. We show that this improvement increases as the pulsation frequency increases, peaking at critical values above which the degree of mixing deteriorates. For very large pulsation frequencies on both inlets ($Re \cdot St > 1$, $Re < 1$), the pulsation period is so small that the winding of the interface between the two streams does not take place, resulting in poor mixing.

The winding of the interface between the two streams is not only dependent on the pulsation frequency, but also on the pulsation amplitude, $\delta V$. An increase in $\delta V/\overline{V}$, the ratio of amplitude over mean or base velocity, is expected to improve the degree of mixing since the length scale of the interface where the two streams meet (and thus the degree of winding) is controlled by $\delta V/f$ in addition to the zone dimensions $W$ and $H$. Larger values of $\delta V/\overline{V}$ are however accompanied by larger temporal fluctuations in the degree of mixing along the mixing channel due to the continuous large amplitude pulsing. In addition, they will result in an increase in the energy consumed, as can be observed from Eq. (13).

Next, results that show the impact on mixing of $\delta V/\overline{V}$, $St$, $Re$, $\phi$, and $H/W$ is presented along with a more detailed discussion based on ANSYS/FLUENT numerical simulations.

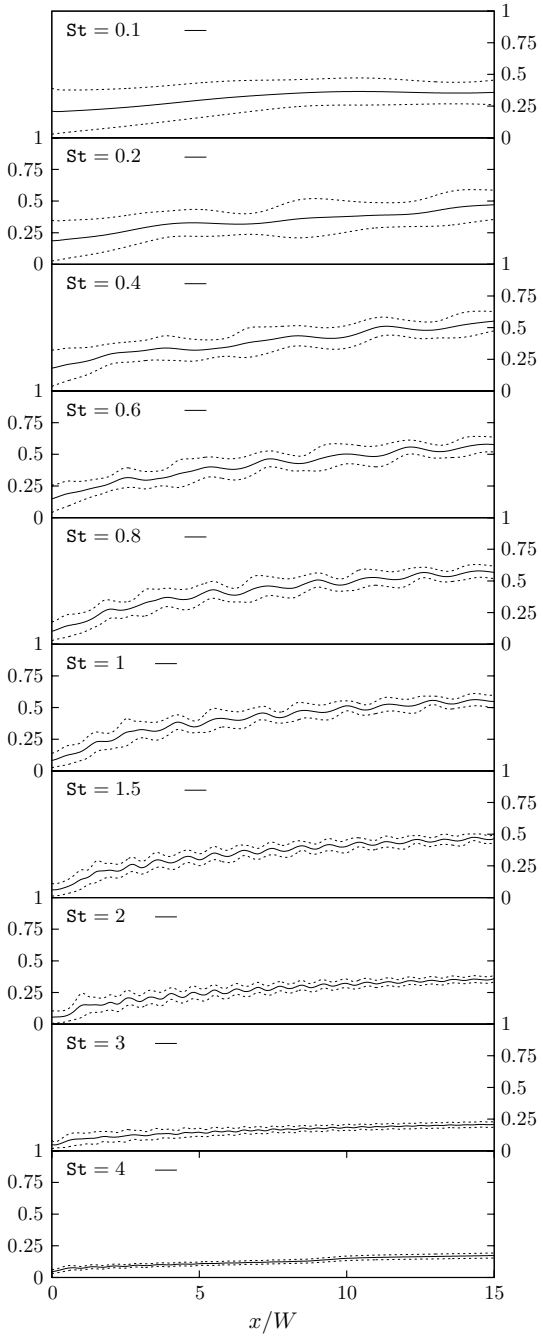


**Fig. 12** Average degree of mixing versus location down the mixing channel at different frequencies and $\delta V/\overline{V} = 5$

### 6.1 Effect of pulsation amplitude

Numerical simulations of the transient mixing of the two pulsating streams were carried for the different values of pulsation amplitude shown in Table 1 for the 2D case where $W = 200\,\mu\text{m}$, $Re = 0.2$, $\phi = 90$, and $St = 2$.

For these different values of $\delta V/\overline{V}$, the degree of mixing versus the location down the mixing the channel is plotted

in Fig. 9 at the quasi-stationary state. The size of the bars on the plot, representing the standard deviation from the average taken over a pulsation cycle, indicates how large the fluctuation in one cycle is at every location. It is evident from Fig. 9 that as $\delta V/\overline{V}$ increases, the mean degree of mixing increases. It is also observed that further down the mixing channel, the fluctuation in the degree of mixing during one quasi-stationary cycle decreases due to the considerable viscous damping encountered in low inertia flows.

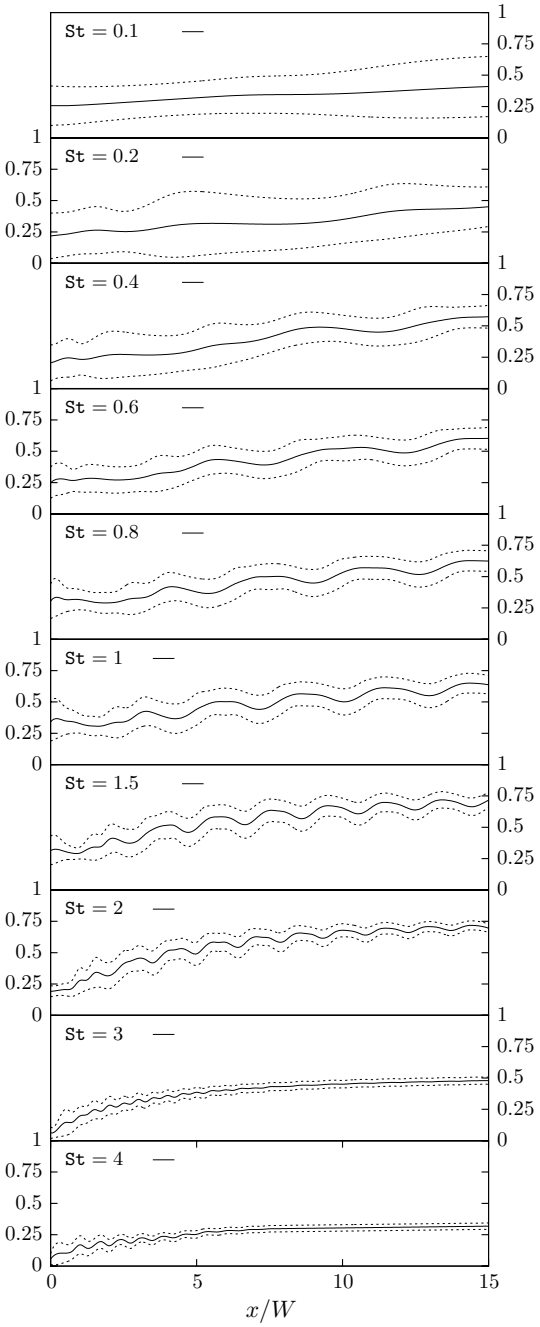


**Fig. 13** Average degree of mixing versus location down the mixing channel at different frequencies and $\delta V/\overline{V} = 7.5$

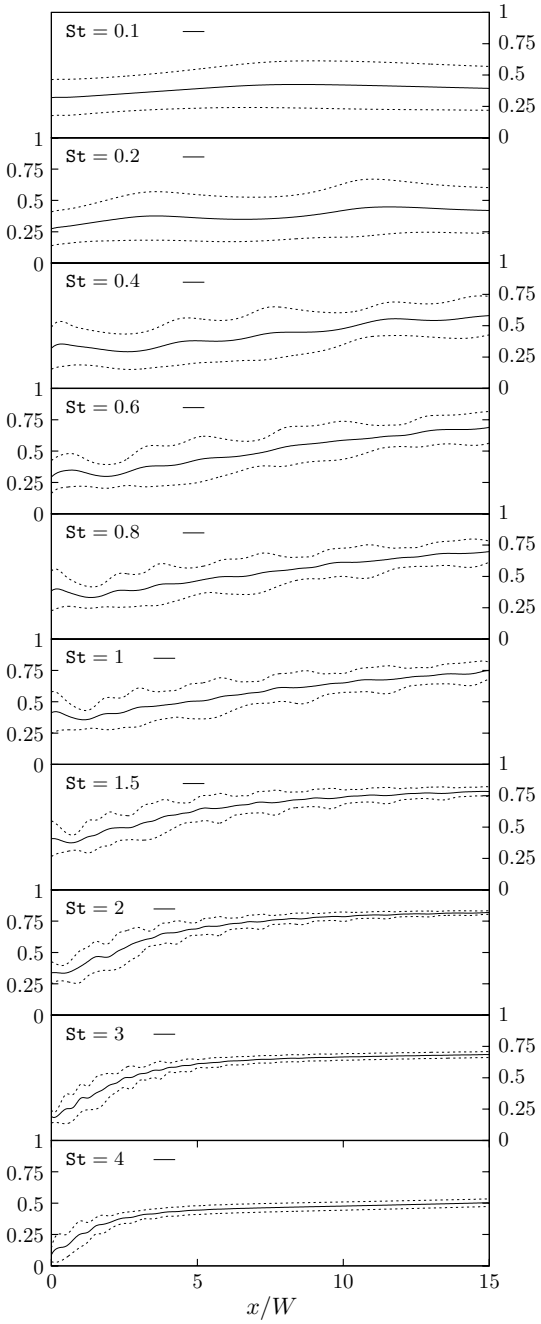


**Fig. 14** Average degree of mixing versus location down the mixing channel at different frequencies and $\delta V/\overline{V} = 10$

Figure 10 plots the average degree of mixing versus $\delta V/\overline{V}$ at four different locations down the mixing channel, showing the standard deviation at the selected points. The results show that the improvement in the average degree of mixing with increasing $\delta V/\overline{V}$ is asymptotic, where at low $\delta V/\overline{V}$ poor mixing is obtained, with the mixing

improving rapidly between $\delta V/\overline{V} = 3.75$ and $\delta V/\overline{V} = 7.5$. For $\delta V/\overline{V} > 7.5$, the slope of the graph starts to decrease indicating less improvement in the degree of mixing. As the pulsation amplitude increases, the amplitude of the temporal fluctuations in the degree of mixing over a quasi-stationary cycle is expected to increase, as confirmed in Fig. 10. It can also be observed from Fig. 10 that for locations down the mixing channel beyond $x/W = 10$ the degree of mixing experiences little change both in terms of the mean and standard deviation. In this case, the minimum mixing length is 10 $W$.

The normalized rate of energy consumed versus mixing length for different values of pulsation amplitude is plotted in Fig. 11, as determined from Eq. (13). From the energy consumption point of view, one can infer from Figs. 10 and 11 that the small increase in the degree of mixing at $x/W = 10$ as the pulsation amplitude ($\delta V/\overline{V}$) is increased from 7.5 to 10 is accompanied by 73 % increase in energy consumption. One can also infer that there is a tradeoff between the mixing length and the pulsation of amplitude. Increasing the pulsation amplitude from 7.5 to 10 caused a reduction of the mixing length from 10$W$ (2000 μm) to 5$W$ (1000 μm) for the same value of the average degree of mixing ($\overline{\mu} = 0.6$). This reduction in the mixing length is, in this case, accompanied by a 16 % increase in the energy consumption.

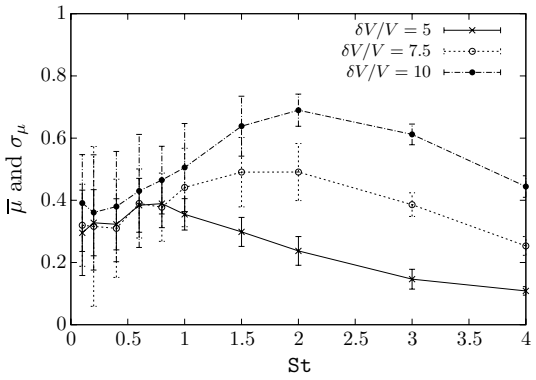


**Fig. 15** Average degree of mixing and the standard deviation versus Strouhal number at $x/W = 5$ for $\delta V/\overline{V} = 5, 7.5$ and 10

### 6.2 Effect of pulsation frequency

To capture the impact of the pulsation frequency on mixing and the associated energy cost, transient simulations were performed for the 2D cases listed in Table 2. The simulations were carried out for three different values of the pulsation frequency $\delta V/\overline{V} = 5$, 7.5 and 10 to allow the investigation of the combined effect of Strouhal number and $\delta V/\overline{V}$. For all the cases considered, $\overline{V} = 0.001$ m/s, $W = 200\,\mu$m, $\phi = 90$, and $Re = 0.2$.

In Figs. 12, 13 and 14, the degree of mixing ($\overline{\mu}$), averaged over a cycle at the quasi-stationary state, is plotted against the location down the mixing channel for three different values of pulsation amplitude; $\delta V/\overline{V} = 5$, 7.5 and 10 respectively. The dotted lines correspond to $\overline{\mu} + \sigma_\mu$ and $\overline{\mu} - \sigma_\mu$. For all the values of $\delta V/\overline{V}$ considered, it can be observed that at the highest frequencies, both the average degree of mixing and the standard deviation are the smallest. At low frequencies, the average degree of mixing is also small, but the standard deviation is the largest. The highest achieved mixing occurs within a certain range of Strouhal numbers for each value of $\delta V/\overline{V}$; below and above which the mixing is worse. This can also be observed in Figs. 15, 16, and 17 where the average degree of mixing and standard deviation, over a cycle at the quasi-stationary state, are plotted versus Strouhal number at the locations $x/W = 5$, 10, and 15 respectively. At each of the locations considered, there is an optimal Strouhal number at which the mixing is highest, and moving away from this optimum

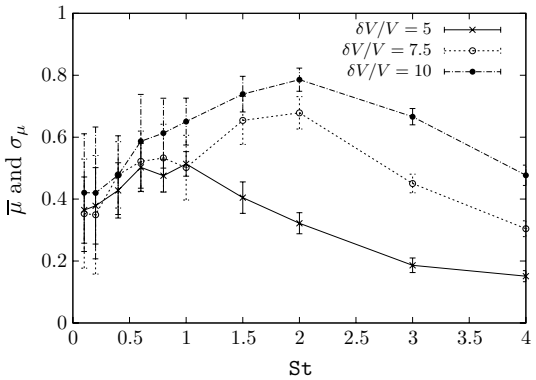


**Fig. 16** Average degree of mixing and the standard deviation versus Strouhal number at $x/W = 10$ for $\delta V/\overline{V} = 5, 7.5$ and 10

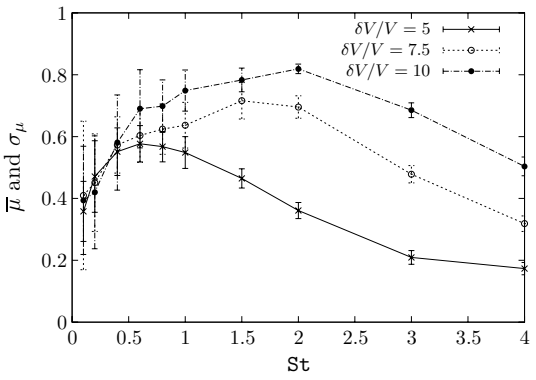


**Fig. 17** Average degree of mixing and the standard deviation versus Strouhal number at $x/W = 15$ for $\delta V/\overline{V} = 5, 7.5$ and 10

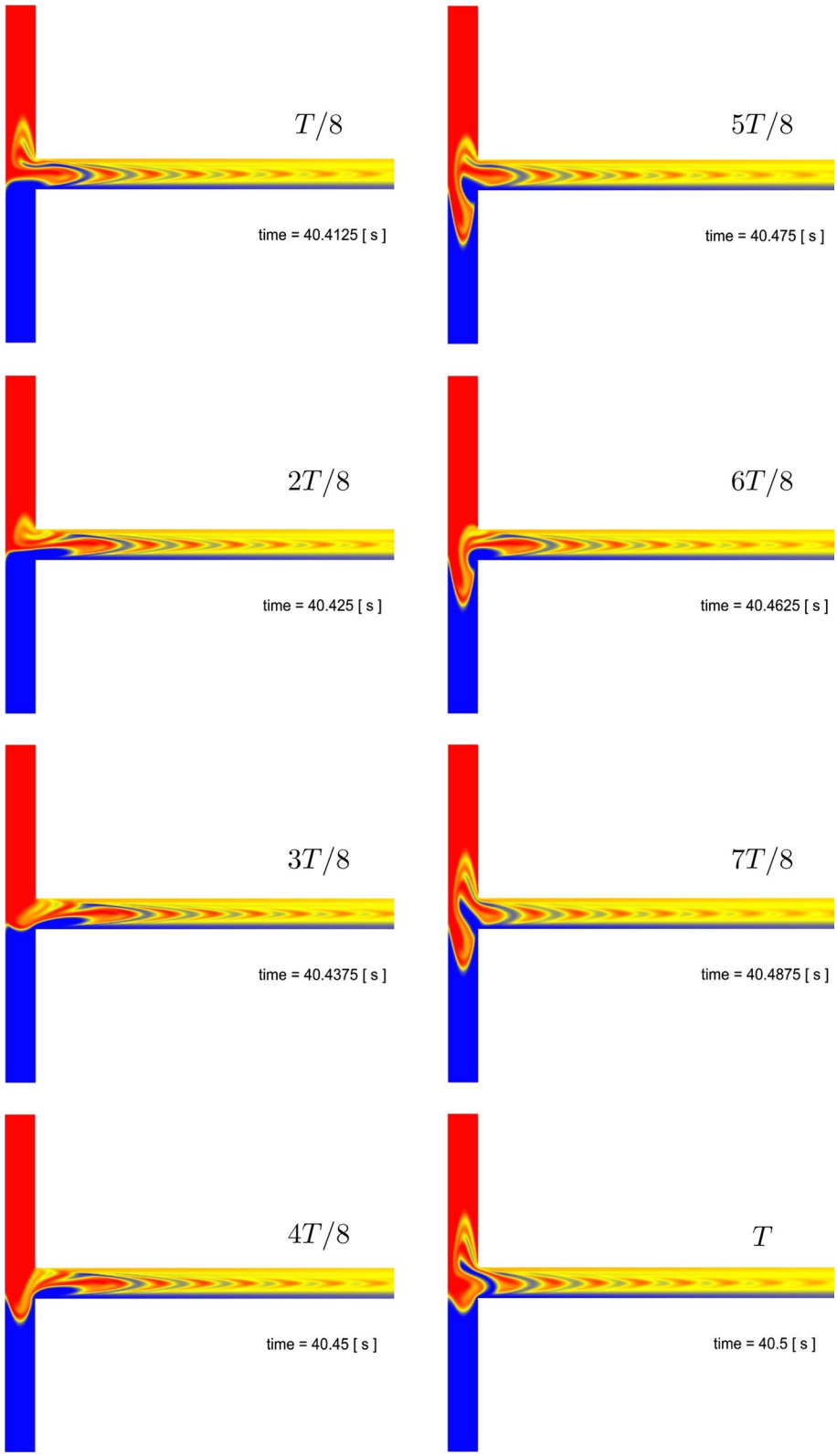


**Fig. 18** Degree of mixing for the case: $St = 2, \delta V/\overline{V} = 10, Re = 0.2$

in both directions will decrease the average degree of mixing. These values of optimum Strouhal numbers for mixing are larger for larger $\delta V/\overline{V}$. The degree of fluctuation over a cycle at the quasi-stationary state, quantified by the size of the bars in Figs. 15, 16, and 17, decreases as the pulsation frequency (or Strouhal number) is increased. In

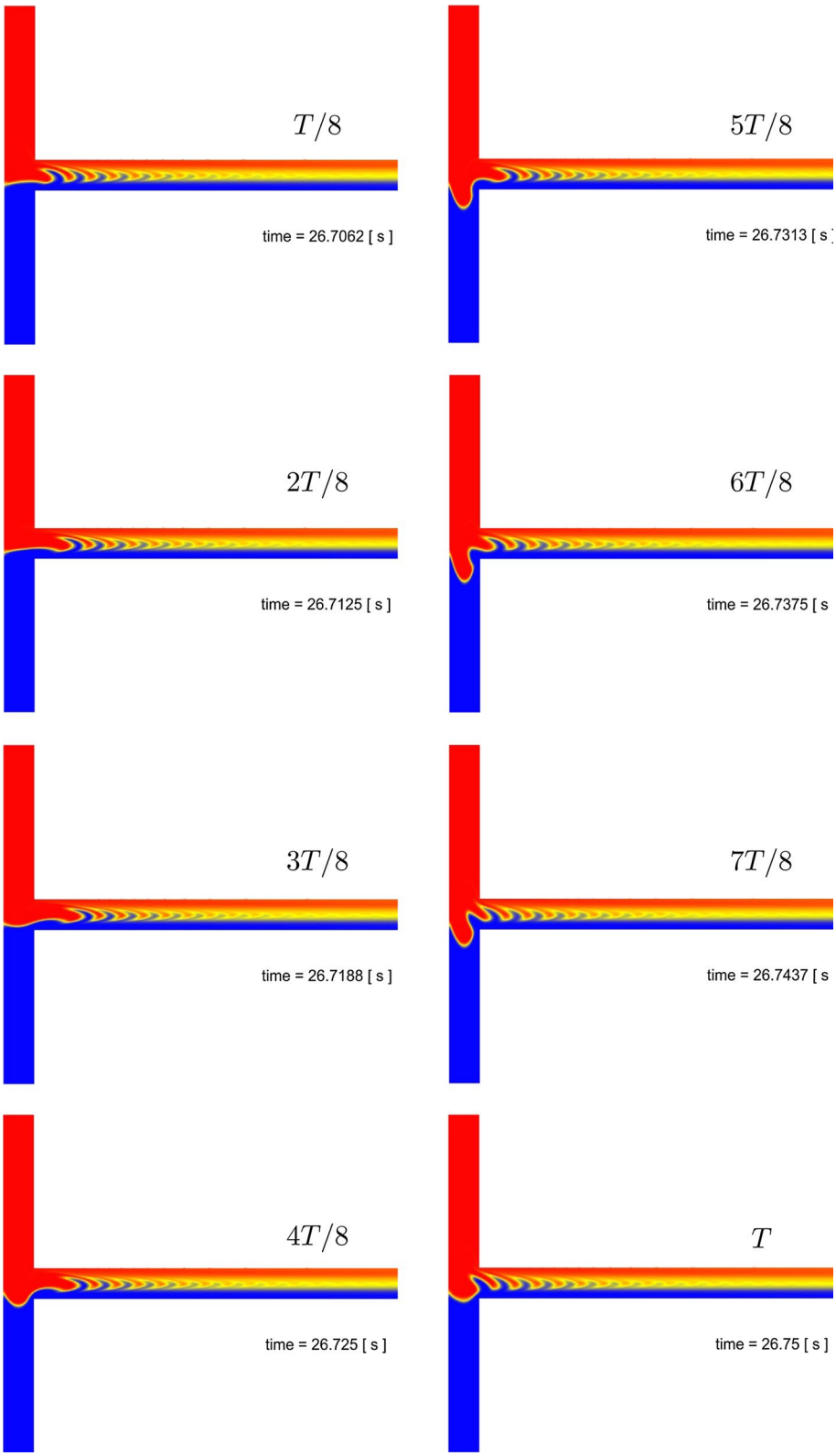


**Fig. 19** Degree of mixing for the case: $St = 4$, $\delta V/\overline{V} = 10$, $Re = 0.2$

some cases, the pulsation frequency that yields the highest degree of mixing for a given mixing length does not yield the smallest fluctuations, and if a smaller $\sigma_\mu$ is desired, then the pulsation frequency has to be increased, which reduces the average degree of mixing. The figures also show that the average degree of mixing increases as the mixing length increases (larger $x/W$), in accordance with earlier observations.

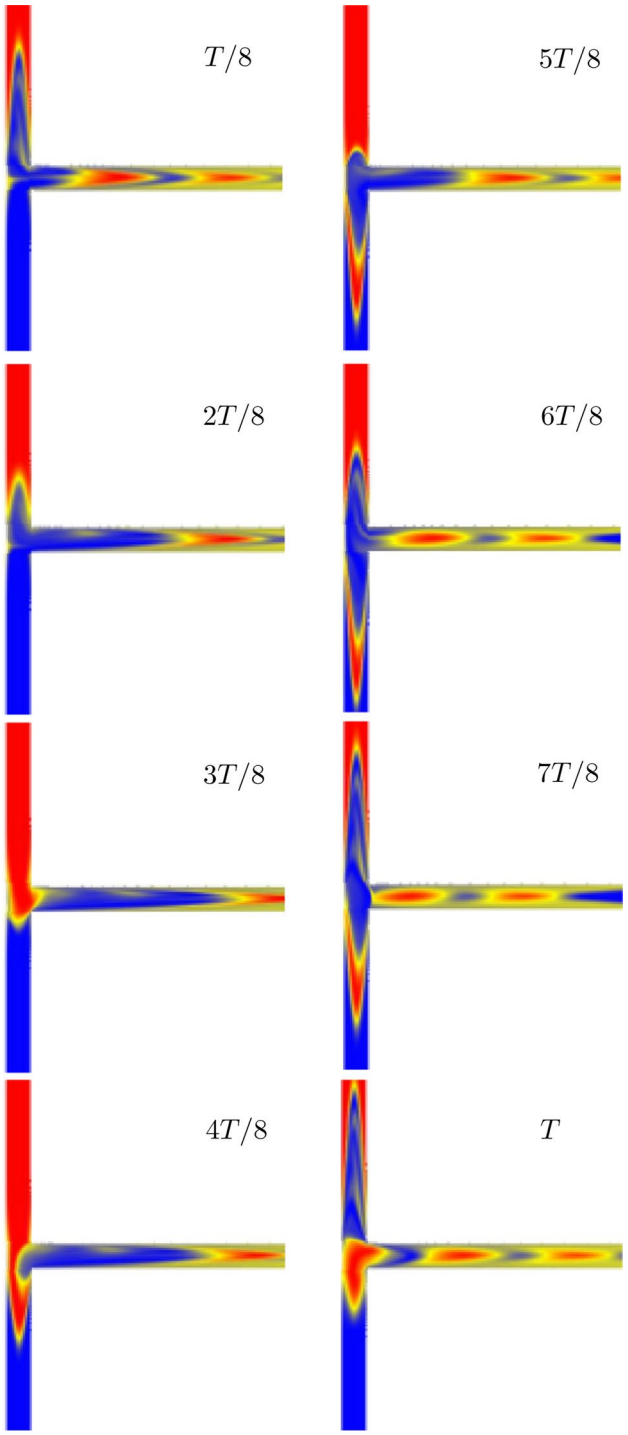


**Fig. 20** Degree of mixing for the case: $St = 0.2$, $\delta V/\overline{V} = 10$, $Re = 0.2$. For visual clarity, the image is magnified three times along the channel width

Figure 18 shows the evolution of the flow during 1 pulsation cycle at $T/8$ intervals for $St = 2$ and $\delta V/\overline{V} = 10$, where the color indicates the species mass fraction: red for mass fraction of 1, blue for mass fraction of 0, and yellow for well-mixed regions of a mass fraction of 0.5. The

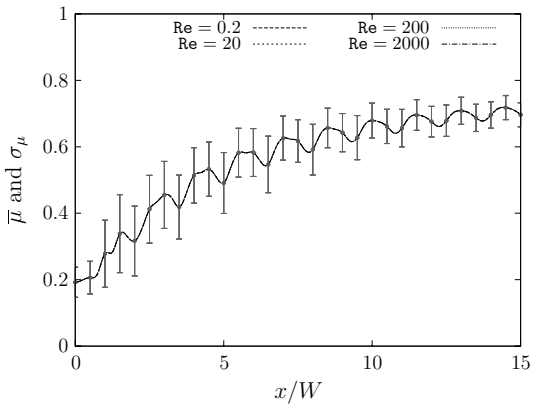


**Fig. 21** Impact of Reynolds number on average degree of mixing and the standard deviation down the mixing channel for $St = 2$ and $\delta V/\overline{V} = 7.5$

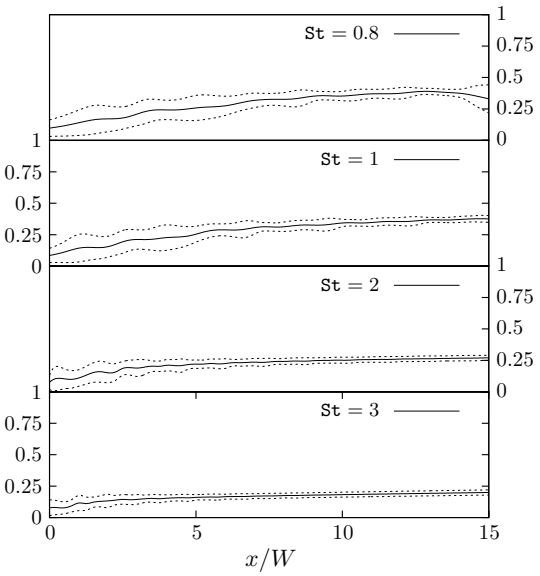


**Fig. 22** Average degree of mixing and standard deviation vs location at $\phi = 45$

pulsing and the change in the interface of the two flows can be seen at the different stages. Figures 19 and 20 show respectively the evolution of the flow at a higher frequency ($St = 4$) and a lower frequency ($St = 0.2$), with the pulsation amplitude kept the same; $\delta V/\overline{V} = 10$. By inspecting the inlet velocity of the two streams, $\overline{V} + \delta V \sin(2\pi ft)$ and $\overline{V} + \delta V \sin(2\pi ft + \pi/2)$, it can be shown that during the first quarter of the pulsation period, both inlet streams flow into the mixing channel. During the second quarter of the pulsation period, the second stream (blue) reverses direction while the first stream (red) continues to flow into the channel at a decreasing speed. During the third quarter of the cycle, both streams flow in the reverse direction (out of

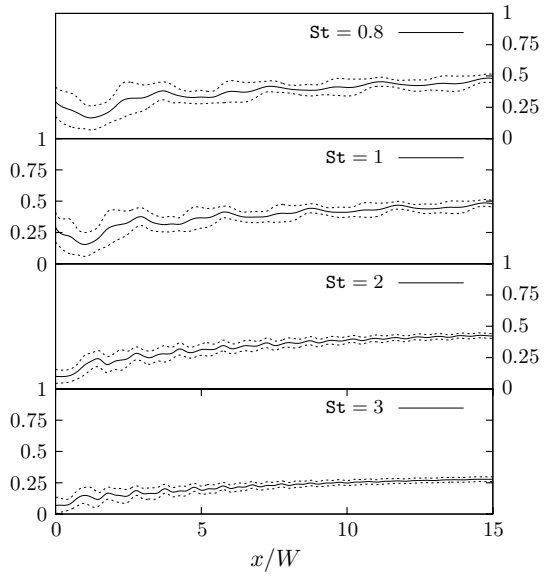


**Fig. 23** Average degree of mixing and standard deviation vs location at $\phi = 135$

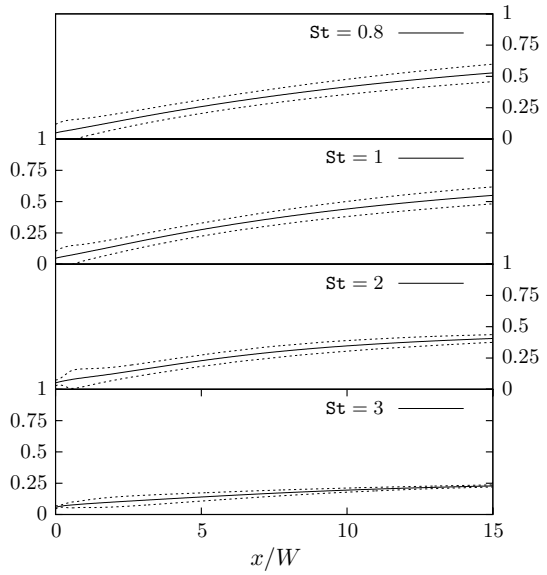


**Fig. 24** Average degree of mixing and standard deviation vs location at $\phi = 180$

the channel). During the last quarter of the pulsation cycle, this first stream continue to flow in the reverse direction at a decreasing speed, while the second stream flows into the channel.

At the low pulsation frequency, the flow down the mixing channel is characterized by alternating zones of fluid from the two inlet streams. For fixed average an pulsation amplitude speeds, the size of these zone is, to a larger degree, determined by the pulsation period. Thus when the

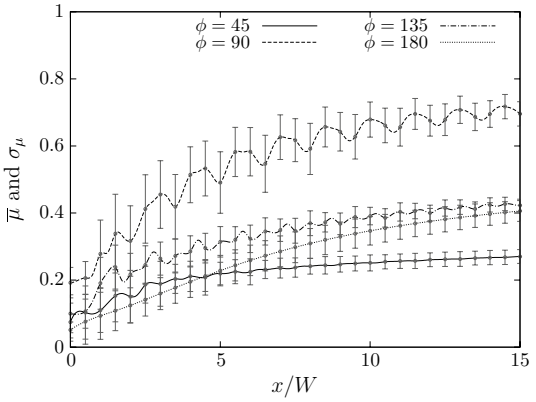


**Fig. 25** Average degree of mixing and standard deviation versus location for different values of $\phi$ and $St = 2$

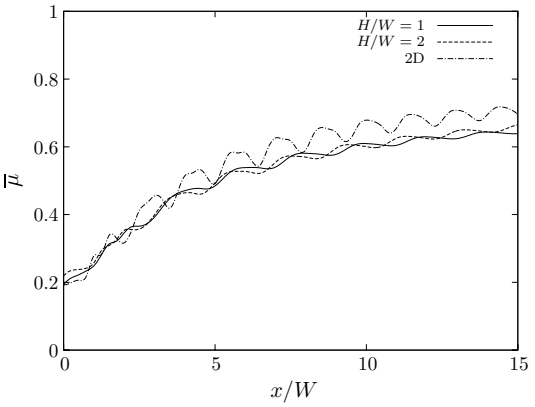


**Fig. 26** Impact of channel aspect ratio on average degree of mixing along the mixing channel for $\delta V/\overline{V} = 7.5$ and $St = 2$

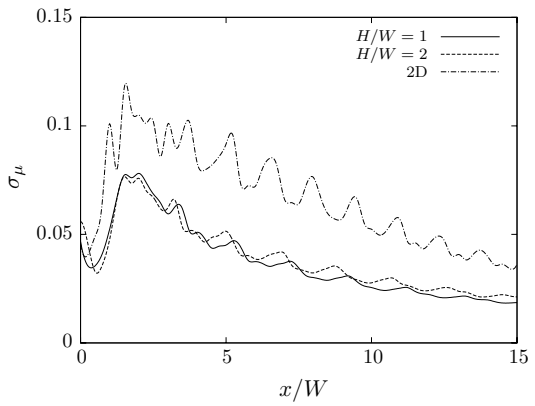


**Fig. 27** Impact of channel aspect ratio on the fluctuation in the degree of mixing (over a quasi-stationary cycle) along the mixing channel for $\delta V/\overline{V} = 7.5$ and $St = 2$

pulsation frequency is small, these alternating zones are significantly longer than $W$, the size of the region where the two streams meet. Mixing in this case occur at the

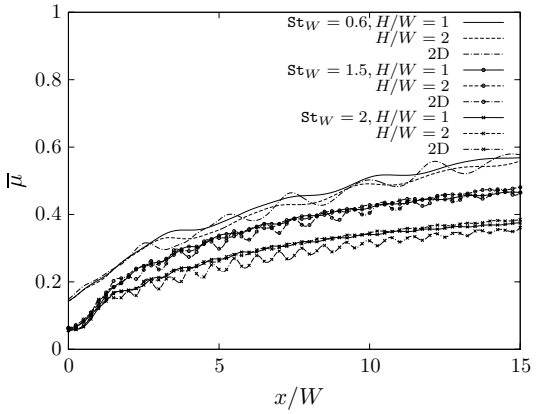


**Fig. 28** Impact of channel aspect ratio on average degree of mixing along the mixing channel for different values of $St$ and $\delta V/\overline{V} = 5$

interface separating these zone, where the length of this interface is approximately $W$ times the number of zones, as can be inferred from Fig. 20. When the pulsation frequency is large, the length scale of the structures produced by the pattern described above is significantly smaller than $W$, and mixing in this case occurs across a winding interface extending downstream the mixing channel, where the winding is characterized by a length scale of the order of magnitude of the pulsation speed times the pulsation period, which is smaller than $W$ when $f \gg \delta V/W$. Optimal mixing occurs at intermediate frequencies, where $\frac{T}{4} \sim \frac{W}{\delta V}$ or $f \sim \frac{\delta V}{4W}$. At this frequency, the winding in the interface between the two streams is of the same order of magnitude as $W$, leading to better mixing per unit length of the mixing channel, as shown in Fig. 18. Mixing of the two streams is thus bounded at both low and high frequencies. At low frequencies the diffusive term is dominated by the advection term, and at high frequencies by the transient term. Both of these effects lead to reduced winding and mass diffusion across the smaller interface between the two streams reduces mixing.

The rate of input work required to overcome friction does not depend on the pulsation frequency, as can be from Eq. (13), where both the viscous and kinetic energy terms on the right-hand side of the equation do not depend on the frequency.

### 6.3 Impact of Reynolds number

Figure 21 shows the impact of Reynolds number on the distribution of the average degree of mixing and the standard deviation (over a cycle at the quasi-stationary state) along the mixing channel for the 2D case with $W = 200\,\mu\mathrm{m}$, $\overline{V} = 0.001$ m/s, and $\phi = 90$. The value of the Reynolds number is varied from 0.2 to 2000 and the flow is considered to be laminar throughout this range. To keep the other dimensionless number constant, Reynolds number is changed by changing the value of the dynamic viscosity, $\eta$. Figure 21 shows that varying the Reynolds number has little effect on the results, where it can be seen that the degree of mixing does not noticeably vary at the different values of $Re$. This is because Reynolds numbers was increased by reducing the viscosity while keeping inlet velocities the same. So while the velocity profile across the mixing channel changes shape as $Re$ is increased, the average velocity is still the same, and consequently Peclet number is the same, where $Pe^{-1} = 0.00025$ indicates that the mixing of the species is strongly limited by mass diffusion.

### 6.4 Impact of phase difference

Impact of the phase difference between the two streams is investigated for phase angles of 45, 90, 135, and 180 for the 2D case with $W = 200\,\mu\mathrm{m}$, $\overline{V} = 0.001$ m/s, $\delta V/\overline{V} = 7.5$, and $Re = 0.2$. Figures 13, 22, 23, and 24 plot the degree of mixing for different Strouhal numbers and phase angles vs $x/W$. Similar to the case studied earlier for $\phi = 90$ (Fig. 13), the fluctuation in the degree of mixing is reduced by increasing Strouhal number and decreases down the mixing channel. Notice that while $St = 2$ is the optimal value for $\phi = 90$, $St = 1$ is optimal for the other phase angles. For $\delta V/\overline{V} = 7.5$, $St = 2$ and $Re = 0.2$, the degree of mixing vs $x/W$ is plotted for the four phase angles in Fig. 25 for $St = 2$. The case of $\phi = 90$ yields the highest values for the degree of mixing, in accordance with the findings in Goullet et al. (2005), 2006), Glasgow et al. (2004), and Glasgow and Aubry (2003).

### 6.5 Effect of sidewalls

In this section, we investigate the effect of sidewalls by comparing the two-dimensional results presented thus far

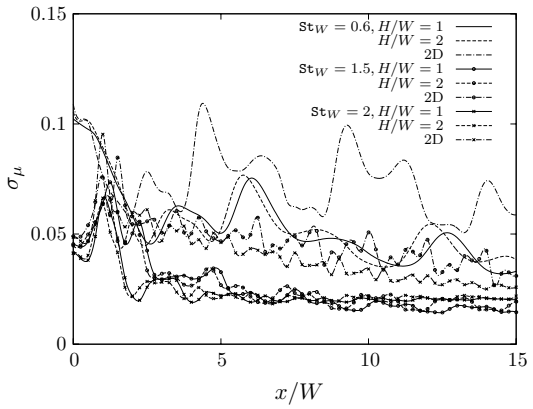


**Fig. 29** Impact of channel aspect ratio on the fluctuation in the degree of mixing (over a quasi-stationary cycle) along the mixing channel for different values of $St$ and $\delta V/\overline{V} = 5$

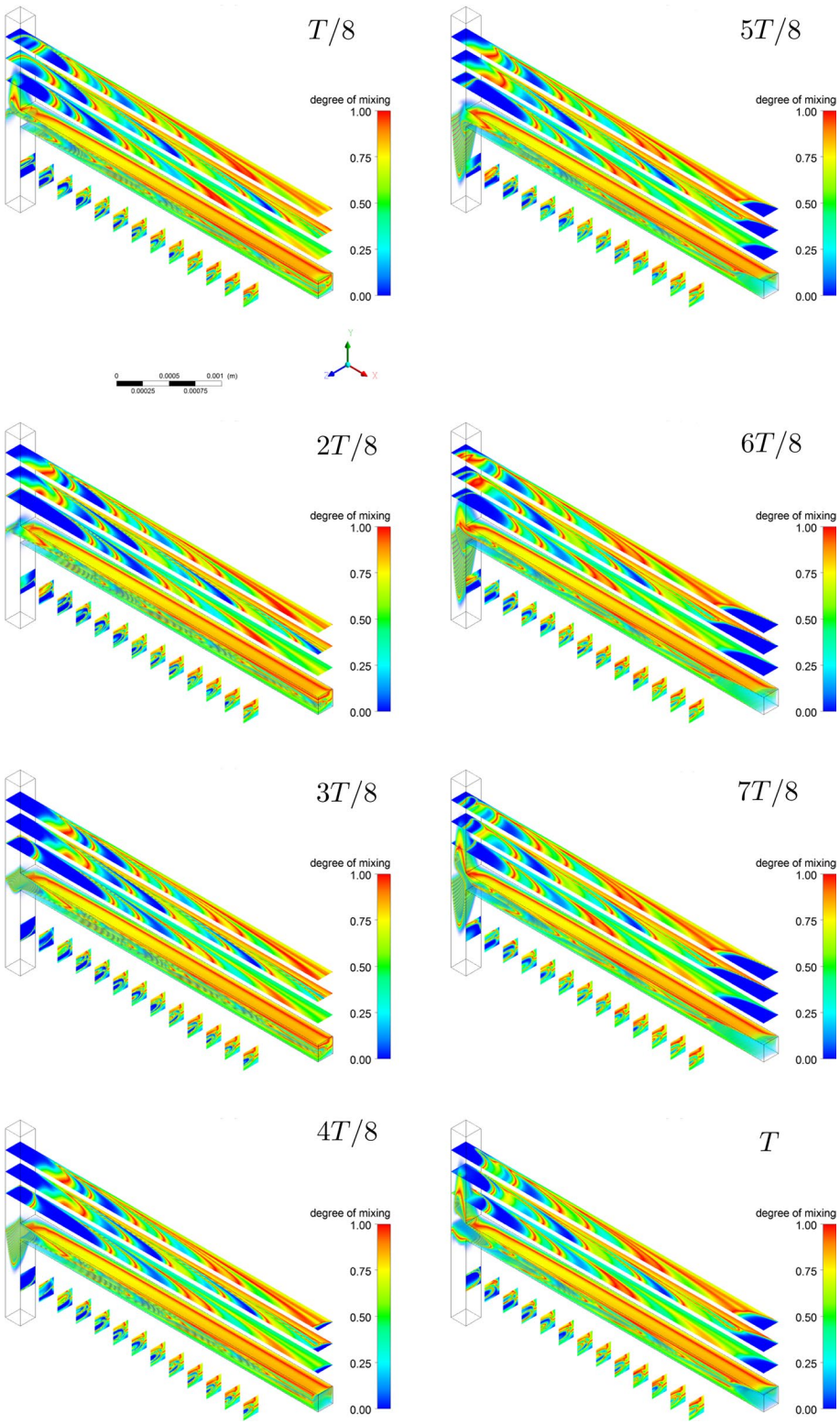


**Fig. 30** Degree of mixing for the 3D case: $H = 400\,\mu\text{m}$, $St = 0.8$, $\delta V/\overline{V} = 5$, $Re = 0.2$

to mixing in 3D channels with $H/W = 1$ and $H/W$=2, $W = 200\,\mu\text{m}$, $\overline{V} = 0.001$ m/s, $Re = 0.2$, and $\phi = 90$. The average degree of mixing along the channel at quasi-stationary state is presented in Fig. 26 for pulsation amplitude and frequency of $\delta V/\overline{V} = 7.5$ and $f = 10$ Hz (corresponding to $St = 2$). The corresponding temporal fluctuations (over one cycle at quasi-stationary state) are plotted in Fig. 27. It can be observed that while the magnitude

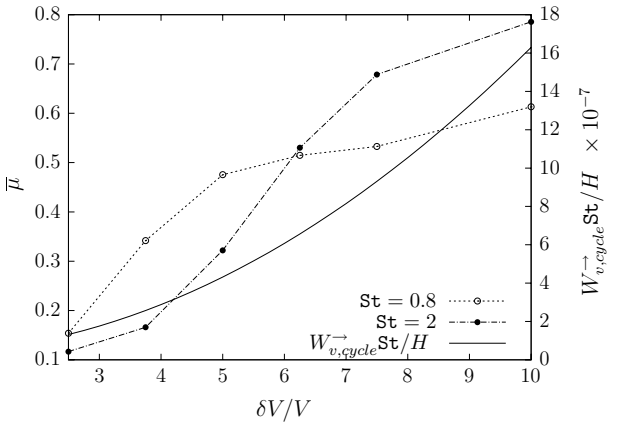


**Fig. 31** Power per unit depth at various *St* at Location $x/W = 10$ down the mixing channel ($L_3 = 2000\,\mu$m)

of the degree of mixing decreases slightly as the height of the channel decreases, both the spatial and temporal fluctuations experience considerable damping owing to the increasing role of friction as a result of the smaller hydraulic diameter. Similar conclusions can be made from Figs. 28 and 29, where the magnitude of the average degree of mixing and the fluctuation are respectively presented for pulsation amplitude of $\delta V/\overline{V} = 5$ and frequencies of $f = 3, 7.5$ and 10 Hz for the three channels.

Figure 30 shows the evolution, at uniformly spaced time intervals of the pulsation period, of the flow for the 3D case with $H = 400\,\mu$m, $St_W = 0.6$, $\delta V/\overline{V} = 5$, and $Re = 0.2$. In addition to the volumetric distribution of the degree of mixing, the figure also displays the degree of mixing distribution at uniformly spaced cross sections along the mixing channel with a spacing of 50$\mu$m. Also shown in the figure are three cross sections along the mixing channel corresponding to $y = -W/4, 0, W/4$.

## 7 Selecting design operation conditions

In selection of design operating conditions, the discussion so far has established that the following needs to be taken into account (1) degree of mixing (spatially averaged over a cross section and temporally averaged over a cycle at the quasi-stationary state), (2) temporal fluctuations in the degree of mixing over one cycle, (3) choice of the mixing length based on (1) and (2), (4) the power required to overcome viscous forces in the mixing channel, and (5) the desired throughput, which is the flowrate exiting the mixing channel. For $\overline{V}_1 = \overline{V}_2 = \overline{V}$, $\delta V_1 = \delta V_2 = \delta V$ and $W_1 = W_2 = W$, the throughput is $2\overline{V}WH$.

For example, if the minimum desired average degree of mixing is 0.5 and maximum fluctuation is 0.05 ($\sigma_\mu \leq 0.05$), then these design requirements can be achieved with (a) $f = 10$ Hz, $\delta V/\overline{V} = 6.25$, with a minimum mixing length of 2150 $\mu$m, or with (b) $f = 10$ Hz, $\delta V/\overline{V} = 10$, with a minimum mixing length of 1500 $\mu$m. In choosing between these two operating points, there is a tradeoff between length of mixing and energy. While the length of the mixing channel for operating point (b) is 70 % less than that in (a), the power cost is twice.

If the fluctuations in the degree of mixing are small, as is the case for channels with smaller *H*/*W*, a chart similar to the one shown in Fig. 31 can be used for selecting design operating conditions for a given length of the mixing channel. The figure illustrates the parabolic dependence of the power per unit length of the channel ($W^{\rightarrow}_{v,\text{cycle}} \cdot f/L_3$) on pulsation amplitude for $Re = 0.2$ and $L_3 = 2000\,\mu$m. Superimposed on the same graph is the degree of mixing versus $\delta V/\overline{V}$ for two values of Strouhal number in the optimal range identified above. Figure 31 can be used to pick the pulsation frequency and amplitude (for a mixing channel of 2000 $\mu$m length) to realize a desired degree of mixing while taking into consideration the power consumption.

## 8 Conclusion

This work presents a numerical study of mixing using pulsating flows in terms of dimensionless numbers that represent the pulsation amplitude ($\delta V/\overline{V}$), pulsation frequency (*St*), phase angle ($\phi$), channel height (*H*/*W*), and fluid viscosity (*Re*). This work also takes into account the rate of work input required to overcome viscous effect and achieve mixing. Over the covered ranges of parameters, the pulsation amplitude ($\frac{\delta V}{\overline{V}}$) and frequency (*St*) proved to have the biggest impact on the degree of mixing down the mixing channel. Both the average and the temporal fluctuations in the degree of mixing over a quasi-stationary cycle are considered. Due to the sensitivity of the solution to various numerical parameters, care has been taken to (1) extend the channel length to account for the effect of the exit boundary conditions during flow reversal, (2) sufficiently resolve space and time, (3) run the simulations long enough to reach a quasi-stationary state. It was found that, due to pulsation, the degree of mixing experiences spatial fluctuations down the mixing channel as well as temporal fluctuation over a pulsation cycle. Larger fluctuations in the degree of mixing over a quasi-stationary cycle are observed at lower frequencies (*St*) and higher pulsation amplitudes ($\delta V/\overline{V}$). For a given *W*, the magnitude of these fluctuations is smaller as $H/W \rightarrow 1$ due to the increasing role of viscous damping. We also found out that there is an optimal pulsation frequency below and above which the mixing deteriorates and that this optimal frequency depends on the pulsation amplitude and channel width as $f \sim \frac{\delta V}{4W}$. For low inertia flows, the rate of work input required to overcome

friction does not depend on the pulsation frequency. As for dependence on the pulsation amplitude, increasing the pulsation amplitude ($\frac{\delta V}{V}$) yields better mixing for a given Strouhal number. This improvement is, however, asymptotic where the large increase in energy cost may not justify the slight improvement in the degree of mixing.

## References


Atkins P, De Paula J (2010) Physical chemistry for the life sciences. Oxford University Press, Oxford

Bessoth F (1999) Microstructure for efficient continuous flow mixing. Anal Commun 36(6):213–215

Capretto L, Cheng W, Hill M, Zhang X (2011) Micromixing within microfluidic devices. In: Microfluidics. Springer, pp 27–68

Chang CC, Yang RJ (2007) Electrokinetic mixing in microfluidic systems. Microfluid Nanofluid 3(5):501–525

Du E, Manoochehri S (2010) Optimal design of microgrooved channels with electrokinetic pumping for lab-on-achip applications. Nanobiotechnol IET 4(2):40–49

Glasgow I, Aubry N (2003) Enhancement of microfluidic mixing using time pulsing. Lab Chip 3(2):114–120

Glasgow I, Lieber S, Aubry N (2004) Parameters influencing pulsed flow mixing in microchannels. Anal Chem 76(16):4825–4832

Goullet A, Glasgow I, Aubry N (2005) Dynamics of microfluidic mixing using time pulsing. Discrete Contin Dyn Syst Suppl 2005:327–336

Goullet A, Glasgow I, Aubry N (2006) Effects of microchannel geometry on pulsed flow mixing. Mech Res Commun 33(5):739–746

Hessel V, Löwe H, Schönfeld F (2005) Micromixers—a review on passive and active mixing principles. Chem Eng Sci 60(8):2479–2501

Issa L (2015) Perturbation-based simplified models for unsteady incompressible microchannel flows. Appl Math Model. doi:10.1016/j.apm.2015.12.025. http://www.sciencedirect.com/science/article/pii/S0307904X15008379

Karniadakis G, Beskok A, Aluru N (2006) Microflows and nanoflows: fundamentals and simulation, vol 29. Springer, Berlin

Knight JB, Vishwanath A, Brody JP, Austin RH (1998) Hydrodynamic focusing on a silicon chip: mixing nanoliters in microseconds. Phys Rev Lett 80(17):3863

Lakkis IA (2008) System-level modeling of microflows in circular and rectangular channels. In: ASME 2008 6th international conference on nanochannels, microchannels, and minichannels. American Society of Mechanical Engineers, pp 1159–1170

Lim Y, Kouzani A, Duan W (2010) Lab-on-a-chip: a component view. Microsyst Technol 16(12):1995–2015

Lu LH, Ryu KS, Liu C (2002) A magnetic microstirrer and array for microfluidic mixing. J Microelectromech Syst 11(5):462–469

Patrascu M, Gonzalo-Ruiz J, Goedbloed M, Brongersma SH, Crego-Calama M (2012) Flexible, electrostatic microfluidic actuators based on thin film fabrication. Sens Actuators A: Phys 186:249–256

Stone HA, Stroock AD, Ajdari A (2004) Engineering flows in small devices: microfluidics toward a lab-on-a-chip. Annu Rev Fluid Mech 36:381–411